JOURNAL OF STRUCTURAL BIOLOGY 113, 148–163 (1994)

Paramyosin Polarity in the Thick Filament of Molluscan Smooth Muscles

NELLY PANTÉ[1]

Rosenstiel Basic Medical Sciences Research Center, Brandeis University, Waltham, Massachusetts 02254

Received September 2, 1994, and in revised form November 21, 1994

Paramyosin is the main structural component of the thick filament of molluscan smooth muscles. These filaments consist of a large paracrystalline core of paramyosin with myosin arranged on its surface. The detailed molecular packing of paramyosin in the core and the array of myosin on the surface of the paramyosin core remain unknown. An unsolved problem is the polarity of the paramyosin molecules within these thick filaments (i.e., it is not known whether the paramyosin molecules assemble with their NH_2-terminal ends pointing toward the center or toward the end of the thick filament). Here a method to distinguish between the NH_2- and the COOH-terminal ends of the paramyosin molecule by electron microscopy is described and used to determine their polarity in synthetic paracrystalline arrays. This method consists of labeling the cysteine residues of paramyosin molecules with the avidin–biotin system developed by Sutoh *et al.* (1984). Accordingly, the sulfhydryl groups of paramyosin—isolated from the anterior byssus retractor muscle (ABRM) of *Mytilus edulis*—were modified with maleimide–biotin, and the biotinylated thiols were visualized in the electron microscope after glycerol spraying/rotary metal shadowing by attaching monomeric avidin to them. Avidin–biotin labeling of the native molecule and its carboxypeptidase fragments revealed that ABRM paramyosin contains one pair of cysteine at its NH_2-terminal end and one pair at ~30 nm from its COOH-terminal end. Synthetic paracrystalline arrays of paramyosin with known axial arrangement were also labeled with the avidin–biotin system. The location of the bound avidin in these paracrystals indicated the polarity of paramyosin in these arrays. The polarity was also determined by comparison of the transverse band-like staining pattern of paracrystals of α-paramyosin (intact protein) and β-paramyosin (a proteolytically cleaved α-paramyosin that has lost a small segment at its COOH-terminal end). Both methods revealed that paramyosin assembles with its NH_2-terminal end pointing toward the center of the paracrystals. The implications of this result for the polarity of paramyosin in the native filament core, and for the arrangement of myosin on the surface of molluscan thick filaments, are discussed. © 1994 Academic Press, Inc.

INTRODUCTION

The thick filaments of invertebrate muscles contain, in addition to myosin, the protein paramyosin, a rod-like coiled-coil molecule similar to the myosin rod (Cohen and Holmes, 1963; Lowey *et al.*, 1963; Kagawa *et al.*, 1989). In contrast to the uniformity observed in vertebrate thick filaments, the thick filaments from invertebrate muscles exhibit considerable variation both in their size and structural organization. This variation seems to be directly related to the content of paramyosin which varies greatly among species and muscle types (reviewed by Bennett and Elliott, 1987). In the smooth adductor muscle of molluscs, where the molar ratio of paramyosin to myosin is three or more (Szent-Györgyi *et al.*, 1971; Levine *et al.*, 1976), the thick filaments are extremely large (up to 100 μm in length and 200 nm in diameter), and paramyosin forms a large paracrystalline core with myosin on the surface (Szent-Györgyi *et al.*, 1971; Nonomura, 1974). In contrast, the thick filaments from one of the fastest invertebrate striated muscles are just 1.8 μm long and contain only a small amount of paramyosin (molar ratio of paramyosin to myosin ≤0.1) which is not assembled in a central core but integrated into the myosin subfilaments (Castellani and Vibert, 1992). Between these two extremes, there are intermediate cases where paramyosin forms a relatively small core which does not exhibit the paracrystalline order present in molluscan smooth muscles. Examples include: (i) the telson muscle of *Limulus* (molar ratio of paramyosin to myosin = 0.5), with ~5-μm-long thick filaments and a small core of paramyosin that does not exhibit any axial repeat (Levine *et al.*, 1982, 1988) and (ii) the thick filaments from the body wall muscle of the

[1] Present address: M. E. Müller-Institute for Microscopy, Biozentrum, University of Basel, Klingelbergstrasse 70, CH-4056 Basel, Switzerland. Fax: 0041-61-267 2259. Bitnet: PANTE@URZ.unibas.ch.

1047-8477/94 $6.00
Copyright © 1994 by Academic Press, Inc.
All rights of reproduction in any form reserved.

nematode *Caenorhabditis elegans* (molar ratio of paramyosin to myosin = 1), which contain a small paramyosin core that does not exhibit the nodal paracrystalline structure seen in molluscs (see below) but reveals a pronounced axial periodicity of 72.5 nm (Deitiker and Epstein, 1993). In these latter muscles, the core of the thick filaments also contains several additional proteins (Epstein *et al.*, 1988; Deitiker and Epstein, 1993).

The molecular packing of paramyosin in the core and the myosin–paramyosin assembly in invertebrate thick filaments have not yet been determined. In the thick filaments of striated invertebrate muscles with only a small amount of paramyosin, the efforts have been focused on determining the structural organization of the myosin moiety (see Kensler and Levine, 1982; Vibert and Craig, 1983; Crowther *et al.*, 1985). In molluscan smooth muscles where paramyosin exhibits the highest level of organization, some models for the molecular packing of paramyosin have been proposed (reviewed by Bennett and Elliott, 1987). In these muscles, paramyosin forms a highly paracrystalline core which reveals a distinctive "checkerboard" pattern of dark-stained nodes when negatively stained samples are visualized in the electron microscope (EM) (Hall *et al.*, 1945; Szent-Györgyi *et al.*, 1971; Nonomura, 1974). This pattern was also inferred from X-ray diffraction patterns of whole adductor muscle and was termed the "Bear–Selby net" (Bear and Selby, 1956). The nodal pattern of the native paramyosin core can be described in terms of a rectangular unit cell, 72.5 nm long and ~30 nm wide, with five equivalent nodes (Bear–Selby nodes) that are axially staggered by 29 nm (i.e., $\frac{2}{5} \times 72.5$ nm). How paramyosin assembles to form such a paracrystalline array has remained elusive.

The finding by Cohen *et al.* (1971) that purified paramyosin could form *in vitro* paracrystalline arrays with the same axial periodicity as that observed with the native paramyosin core helped to explain the Bear–Selby net. Provided that the protein has been solubilized in urea and/or KSCN, paramyosin forms a variety of paracrystalline arrays in the presence of divalent cations. These paracrystals exhibit different bright–dark transverse banding patterns when negatively stained samples are examined in the EM (Cohen *et al.*, 1971), but all of them reveal an axial periodicity of 72.5 nm. The simplest banding pattern, called the P1 array, consists of ~52.5-nm-wide bright staining bands separated by an ~20-nm-wide dark band. Cohen *et al.* (1971) interpreted these staining patterns in terms of an axial gap/overlap arrangement of paramyosin molecules. Accordingly, the dark regions represent gap areas where stain can penetrate, and the bright regions represent the overlap areas from where stain is excluded. The same authors further demonstrated that the P1 paracrystal is the basic array which accounts for the other *in vitro* paracrystalline forms and for the Bear–Selby net of the native thick filaments. The paramyosin core was pictured by Cohen *et al.* (1971) to be made up of subfilaments corresponding to the P1 array. Axial displacement of subfilaments by 29 nm thus produces the Bear–Selby net. Therefore, the nodes of the Bear–Selby net correspond to the dark regions of the P1 array, and they represent the gap regions between the ends of adjacent paramyosin molecules. Based on these findings, Elliott and Bennett (1984) proposed a model for the packing of paramyosin in the thick filament consisting of stacked layers of molecules each having the two-dimensional structure of the Bear–Selby net. This model is supported by the following observations: (i) 3-D reconstruction of tilted thick filaments revealed that the stain in the Bear–Selby nodes extended like bars throughout the depth of the filament (Dover and Elliott, 1979); and (ii) transverse sections of molluscan muscles revealed a striped pattern on the thick filaments (Elliott, 1964; Bennett and Elliott, 1981). These results indicate that the native paramyosin core has a crystal-like structure. It is difficult, however, to understand how a filament with cylindrical geometry (i.e., revealed by round cross sections and tapered ends) could comprise a single crystal. Thus, it has remained elusive how paramyosin is packed in the core of the thick filament of molluscan smooth muscles.

The arrangement of myosin on the paramyosin core of molluscan thick filaments is another unsolved problem that has been difficult to resolve because the myosin tends to disassemble during EM preparation of the thick filaments (Nonomura, 1974). However, models in which myosin forms a uniform layer one (Cohen, 1982) or two (Squire, 1973) molecules thick have been proposed. In these models, it is assumed that the arrangement of the myosin molecules on the surface of the paracrystalline paramyosin core is governed by the packing of the paramyosin molecules. However, Castellani *et al.* (1983) found that in the pedal retractor muscle of *Mytilus edulis* (molar ratio paramyosin to myosin = 1), the myosin molecules are helically arrayed on the surface of the nodal paramyosin core with no evident relationship between the two arrays.

One basic aspect of the molecular packing within the native paramyosin core that remains to be resolved is the polarity of the molecule. Specifically, it is not known whether the paramyosin molecules assemble with their NH_2-terminal ends pointing toward the center or toward the end of the filament. Since myosin in the thick filament assembles in a bipolar fashion with the NH_2-terminal ends (i.e., the myosin heads of the molecules) pointing toward the

end of the filament, it is expected that paramyosin forms a bipolar core. This bipolarity is revealed by the polarity of the Bear–Selby nodes: they have a roughly triangular shape with one vertex pointing toward the center of the filament (Szent-Györgyi *et al.*, 1971). This orientation has been reported to be the same in different species (Bennett and Elliott, 1984).

In vitro, paramyosin self-assembles into both polar and bipolar paracrystals (Cohen *et al.*, 1971). Some information about the polarity of paramyosin within these paracrystals has been obtained by Weisel (1975). He compared *in vitro* formed paracrystalline arrays of earthworm paramyosin with those of the carboxypeptidase-treated molecule and found that the central regions of both intact and digested paramyosin paracrystals revealed the same staining pattern. He concluded that the central region of these paracrystals represents an overlap between the NH_2-terminal ends of the molecules and that paramyosin assembles with this end pointing toward the center of the paracrystal. Presumably, paramyosin assumes the same orientation in the thick filament, i.e., the NH_2-terminal end pointing toward the center of the filament. This orientation for the paramyosin molecule would imply that in the native thick filament myosin and paramyosin would coassemble in an antiparallel fashion, where the NH_2-terminal end of paramyosin interacts with the COOH-terminal end of myosin. However, Kagawa *et al.* (1989), using results from electrostatic interactions between the amino acid sequence of paramyosin and that of the myosin rod from *C. elegans,* found that parallel assemblies between these two molecules are favored by interactions between charge clusters spaced periodically in both sequences. Based on these results, these authors proposed a model for the arrangement of myosin and paramyosin in the native thick filament in which the COOH-terminal end of paramyosin points toward the center of the filament, an orientation opposite to that found in synthetic paracrystalline arrays of paramyosin (Weisel, 1975). Thus, the polarity of paramyosin in the native thick filament has remained elusive.

In the present study, the avidin–biotin system developed by Sutoh *et al.* (1984) was used to distinguish between the NH_2- and the COOH-terminal end of paramyosin by EM. This method was used to determine the polarity of paramyosin in paracrystalline arrays. The polarity was also determined by comparing the transverse band-like staining pattern of paracrystals of α-paramyosin (the native molecule) with those of β-paramyosin (a proteolytically cleaved α-paramyosin that has lost a small segment of the COOH-terminal end). The results of both studies reveal that paramyosin assembles with the NH_2-terminal end pointing toward the center of the filament, thus being consistent with the earlier finding by Weisel (1975).

MATERIALS AND METHODS

Live *M. edulis* mussels were obtained from local fish markets. All chemicals used were of analytical grade. Avidin, carboxypeptidase A (DFP-treated), carboxypeptidase G, trypsin, maleimide–biotin, the Ellman reagent (5,5′-dithio-bis(2-nitrobenzoic acid); DTNB), and the protease inhibitors (leupeptin, pepstatin A, phenylmethylsulfonyl fluoride (PMSF), tosyllysine chloromethyl ketone (TLCK), tosylphenylalanine cloromethyl ketone (TPCK), and soybean trypsin inhibitor) were obtained from Sigma (St. Louis, MO). DEAE-Sephadex was from Pharmacia (Uppsala, Sweden). All procedures were performed at 4°C unless otherwise stated.

Paramyosin Preparation

α-Paramyosin (the native form) was prepared from the anterior byssus retractor muscle (ABRM) of *M. edulis* by the ethanol precipitation method of Johnson *et al.* (1959), with the modification introduced by Stafford and Yphantis (1972), followed by ion exchange chromatography on DEAE-Sephadex. Briefly, freshly dissected muscles were homogenized in EDTA–wash buffer (40 m*M* NaCl, 10 m*M* EDTA, 3 m*M* NaN_3, 0.1 m*M* PMSF, 0.1 m*M* DTT, 1 μg/ml leupeptin, 1 μg/ml pepstatin A, 10 m*M* sodium phosphate, pH 7.0) with a Sorvall omnimixer and washed three times in the same buffer. Paramyosin was extracted from this homogenate with high-salt buffer (0.6 *M* NaCl, 10 m*M* EDTA, 3 m*M* NaN_3, 1 m*M* DTT, 5 m*M* sodium phosphate, pH 7.6). Three volumes of 95% ethanol containing 1 m*M* DTT were added to the soluble extract, and the precipitated paramyosin and denatured actomyosin were collected by centrifugation (10 000*g* for 20 min). The pellet was resuspended in high-salt buffer and dialyzed overnight at 4°C against the same buffer. Soluble proteins (i.e., the supernatant after centrifugation at 10 000*g* for 20 min) were dialyzed against low-salt buffer (40 m*M* NaCl, 10 m*M* EDTA, 3 m*M* NaN_3, 1 m*M* DTT, 5 m*M* sodium phosphate, pH 6.0) and washed three times in the same buffer to remove tropomyosin. The precipitate of crude paramyosin was resuspended in a small volume of high-salt buffer and clarified by centrifugation at 50 000*g* for 1 hr.

By gel electrophoresis (SDS–PAGE) this preparation was found to contain a contaminant of 110 kDa (i.e., a degradation product of myosin; Castellani *et al.*, 1988). To remove this contaminant, a batch method involving ion exchange chromatography on DEAE-Sephadex was developed. The paramyosin preparation was incubated with DEAE-Sephadex in 40 m*M* sodium pyrophosphate, 10 m*M* NaCl, 10 m*M* EDTA, pH 7.8, for 20 min. Under these conditions, the contaminant bound to the DEAE-Sephadex while the paramyosin remained in solution. The pure paramyosin was then separated by centrifugation (18 000 rpm for 20 min). The paramyosin was concentrated by dialysis in low-salt buffer, centrifuged and resuspended in high-salt buffer. This paramyosin could be stored for a few days on ice. For long-term storage, the protein was dialyzed against 0.6 *M* ammonium bicarbonate, pH 7.6, 1% sucrose and lyophilized.

All buffers used during the purification procedure contained 10 m*M* EDTA and leupeptin and pepstatin A at 1 μg/ml in order to minimize degradation of native α-paramyosin. β-Paramyosin (proteolytically cleaved α-paramyosin that has lost a segment of the COOH-terminal end; Yeung and Cowgill, 1976) was prepared by the same method but the extraction of the myofibrils and the ethanol precipitation were done at room temperature and the buffers used did not contain EDTA or proteolytic inhibitors (Stafford and Yphantis, 1972).

Carboxypeptidase Digestion

α-Paramyosin at 2 mg/ml in 0.6 *M* NaCl, 50 m*M* Tris–Cl, pH 8.0, was treated with 1% carboxypeptidase A (DFP-treated) or

carboxypeptidase G dissolved in the same buffer and containing 0.1 m*M* PMSF, 0.1 m*M* TLCK, 0.1 m*M* TPCK, 10 μg/ml soybean trypsin inhibitor, 1 μg/ml leupeptin, and 1 μg/ml pepstatin A in order to inhibit any contaminant proteases. The reaction was carried out at 0, 25, or 32°C for 2 to 48 hr. Aliquots were removed after 2, 4, 8, 12, 24, and 48 hr of incubation, and the digestion was terminated by adding 10 m*M* EDTA. The samples were then analyzed on 8% SDS–polyacrylamide gels.

Paracrystal Preparation

Paracrystals of α- and β-paramyosin were produced by the procedure described by Cohen *et al.* (1971) which required the presence of 50 m*M* divalent cations as a precipitating agent. Paramyosin at 2 mg/ml in high-salt buffer (see above) was dialyzed first against dispersing buffer (i.e., 1 *M* urea or 100 m*M* KSCN, 50 m*M* Tris–Cl, pH 8.0) and then against precipitating buffer (i.e., 50 m*M* $MgCl_2$ $BaCl_2$, or $CaCl_2$, 50 m*M* Tris–Cl, pH 8.0). In addition, spermine was also used as a precipitating agent (Phillips *et al.*, 1987). In this case, paramyosin at 2 mg/ml was first dialyzed against 0.2 *M* spermine, 50 m*M* Tris–Cl, pH 8.0, a condition which rendered paramyosin soluble, and then against 50 m*M* spermine, 20 m*M* Tris–Cl, pH 8.0.

Determination of SH (Sulfhydryl) Groups

The number of sulfhydryl groups was determined using DTNB by the Ellman method (Ellman, 1959). α-Paramyosin in 8 *M* urea, 50 m*M* Tris–Cl, pH 8.0, was mixed with a 10-fold excess of DTNB. The reaction was set up in matched cuvettes containing equal concentrations of DTNB, and A_{412} was measured. The number of SH groups per paramyosin molecule was calculated using the molar extinction coefficient of DTNB of 13 600 M^{-1} cm^{-1} (Ellman, 1959).

Avidin–Biotin Labeling

α-Paramyosin and carboxypeptidase (A and G) fragments of paramyosin were avidin–biotin labeled by the method developed by Sutoh *et al.* (1984). The protein samples in high-salt buffer (0.6 *M* NaCl, 10 m*M* sodium phosphate, pH 7.6) were first incubated with 10 m*M* DTT for 2 hr in order to reduce the thiol groups and then dialyzed for 6 hr against high-salt buffer containing 0.01 m*M* DTT in order to eliminate the excess of DTT. The reduced samples were then mixed with maleimide–biotin (dissolved in DMSO) at a molar ratio of 1.2:1 (i.e., mal–biotin per total SH groups). After overnight incubation at 4°C, the biotinylated protein was dialyzed against high-salt buffer to eliminate excess reagent. Avidin, dissolved in high-salt buffer (see above), was added to the sample at a molar ratio of 1:1 (avidin per total SH groups). After incubating at 0°C for 4 hr, the avidin–protein complex was examined in the electron microscope (EM) using glycerol spraying/rotary metal shadowing (see below).

Paracrystals of ABRM α-paramyosin were also labeled by this method. In this case, the paracrystals were kept in the precipitating buffer where all the reactions were carried out. The avidin-biotinylated paracrystals were examined in the EM after negative staining (see below).

Isolation of Native Thick Filaments and Preparation of Paramyosin Core

Thick filaments from ABRM were isolated by the method described by Castellani *et al.* (1983). Briefly, freshly dissected ABRM muscles were chemically skinned in a solution containing 50 m*M* NaCl, 5 m*M* $MgCl_2$, 0.5 m*M* EGTA, 5 m*M* ATP, 20 m*M* Mes, pH 7.0, 0.1% saponin for 3 hr. The muscles were then washed in the same solution without saponin and gently homogenized in the same buffer containing 1 m*M* ATP. A drop of the filament suspension was placed on a carbon coated copper grid for 5 min and negatively stained (see below). Paramyosin cores were prepared by the procedure described by Szent-Györgyi *et al.* (1971) as follows: after adsorption of freshly isolated thick filaments on an EM grid, the grid was rinsed with a solution containing 0.4 *M* NaCl, 5 m*M* $MgCl_2$, 1 m*M* ATP, 20 m*M* Mes, pH 6.0, before being negatively stained.

SDS–PAGE and Protein Concentration

SDS–polyacrylamide gel electrophoresis (SDS–PAGE) was performed as described by Laemmli (1970) on either 8 or 5% polyacrylamide gels. The gels were stained with Coomassie brilliant blue R-250. Protein concentrations were determined either by the Lowry method (Lowry *et al.*, 1951) or by the Bradford colorimetric method (Bradford, 1976).

Electron Microscopy

Negative staining. A drop of the paracrystal suspension was adsorbed for 60 sec to a carbon-coated 400-mesh-per-inch copper EM grid. Next the grid was washed with the sample buffer (i.e., the same buffer in which the paracrystals were formed) before being stained with 1% aqueous uranyl acetate.

Glycerol spraying/rotary metal shadowing. Samples were diluted into 0.45 *M* ammonium acetate containing 70% glycerol and sprayed at room temperature onto freshly cleaved mica according to the method of Shotton *et al.* (1979). The mica was then placed in an Edwards evaporator and rotary-shadowed with platinum/carbon at an elevation angle of 6°. Electron micrographs were recorded using either a Philips EM301 or a Philips EM420 electron microscope operated at 80 kV. The magnification was calibrated using negatively stained tropomyosin paracrystals having an axial repeat of 39.5 nm (Caspar *et al.*, 1969).

RESULTS

Characterization of ABRM Paramyosin

When isolating paramyosin from the ABRM of *M. edulis* by standard procedures (Hodge, 1952; Johnson *et al.*, 1959; Szent-Györgyi *et al.*, 1971), a 110-kDa contaminant (which can account for up to 50% of the preparation) was always present (see Fig. 1a, lane 2). This contaminant has previously been identified as a degradation product of myosin which contains the myosin rod domain (Castellani *et al.*, 1988). Hence, the 110-kDa contaminant is also a rod-like molecule with a length very close to that of paramyosin, which could represent a problem in the localization of the SH groups of paramyosin by EM (see below). Therefore, the first step in this investigation was to develop a purification procedure of ABRM paramyosin which eliminates this contaminant. The myosin–rod contaminant was removed by ion exchange chromatography using a batch method with DEAE-Sephadex (see Materials and Methods). ABRM paramyosin obtained by this procedure migrates as a single band with an apparent molecular weight of 100 kDa by SDS–PAGE (Fig. 1a, lane 3). As illustrated in Fig. 1b, when ABRM paramyosin isolated by this method was visualized in the EM after glycerol spraying/rotary metal shadowing, it appears as a rod-like molecule with a contour length of 124.0 ± 1.2 nm (mean ± SD).

Like paramyosin from other species, ABRM

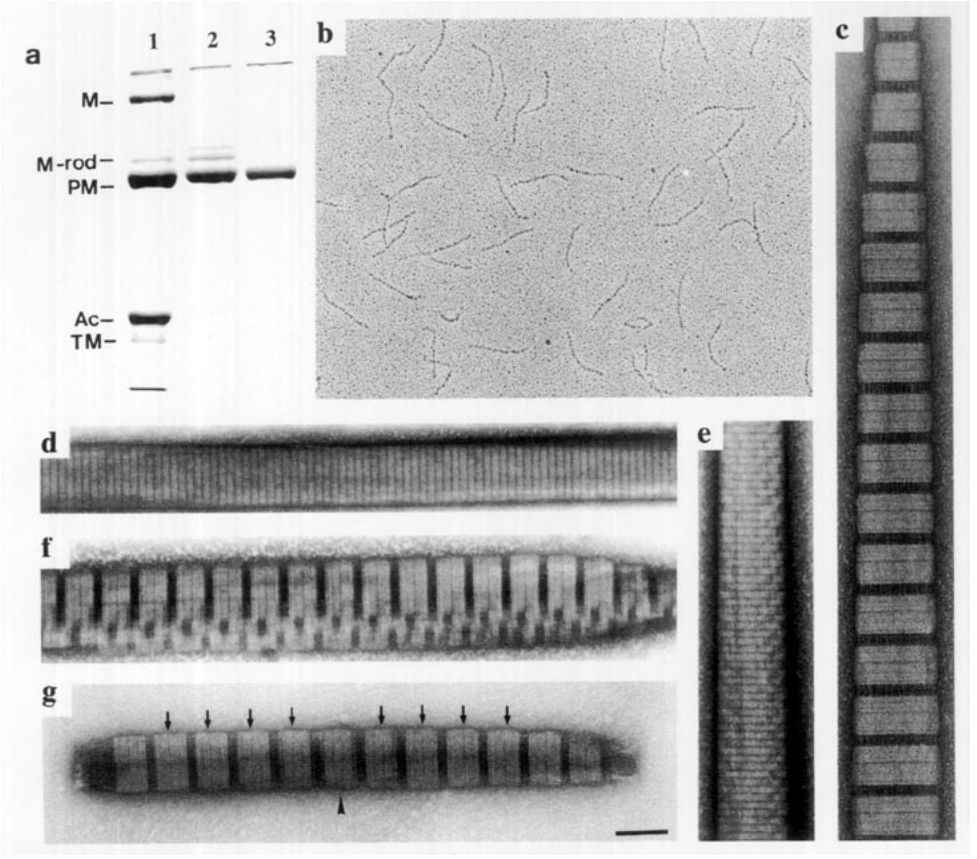

FIG. 1. Characterization of ABRM paramyosin. (a) 8% SDS–polyacrylamide gel of ABRM myofibrils (lane 1) and paramyosin purified by the ethanol precipitation method (Johnson *et al.*, 1959) (lane 2) and by the ion exchange chromatography method (see Materials and Methods) which eliminates the 110-kDa fragment of the myosin rod (lane 3). (M, myosin heavy chain; M-rod, myosin rod contaminant; PM, paramyosin; Ac, actin; TM, tropomyosin). (b) Field of ABRM paramyosin visualized in the EM after glycerol spraying/rotary metal shadowing. (c–f) Negatively stained paracrystals of ABRM paramyosin obtained using 50 m*M* divalent cations (Mg^{2+} or Ca^{2+} or Ba^{2+}) as the precipitating agent. (g) Negatively stained paracrystal of ABRM paramyosin obtained using spermine as the precipitating agent. All the paracrystals exhibited bright–dark transversal staining patterns with an axial periodicity of either 14.5 (d and e) or 72.5 nm (c, f, and g). The paracrystal in c shows the characteristic P1 array which was the most common form. The paracrystals in e and f exhibit some features of the Bear–Selby net of the native thick filaments; for example, the paracrystal in f is a transition form in which two subfilaments having the P1 paracrystalline packing are staggered by 29 nm (i.e., $\frac{2}{5} \times 72.5$ nm). The spermine paracrystal in g exhibits the characteristic P1 band pattern and is bipolar: it has a central 43-nm-wide bright band (arrowhead) where the staining patter change its polarity as indicated by the position of the fine stain lines in the bright/overlap region (arrows). Bar, 100 nm (b, d–g) and 72.5 nm (c).

paramyosin also forms a variety of *in vitro* paracrystalline arrays upon dialysis of the urea or KSCN solubilized protein into a buffer containing 50 m*M* divalent cations (Mg^{2+} or Ca^{2+} or Ba^{2+}). As illustrated in Figs. 1c to 1f, when viewed in the EM after negative staining, these paracrystals were extremely long (>2 μm) and exhibited different bright–dark transverse banding patterns with an axial periodicity of either 14.5 nm (Figs. 1d and 1e) or 72.5 nm (Figs. 1c and 1f). The most common paracrystal form obtained exhibited the characteristic P1 band pattern (Cohen *et al.*, 1971), which, as illustrated in Fig. 1c, consist of ~52.5-nm-wide bright bands separated by an ~20-nm-wide dark band. Some times the paracrystals induced by divalent cations shown some features of the Bear–Selby net of the native thick filament. For example, the paracrystal shown in Fig. 1e exhibited a nodal pattern at its right edges. Similarly, as documented in Fig. 1f, some of the P1 paracrystals shown P1 subfilaments staggered by 29 nm as in the Bear–Selby net.

When 50 m*M* divalent cations were used to induce paracrystal formation, different paracrystal forms were obtained which coexisted even within the same preparation. This paracrystal polymorphism was reduced when spermine was used as the precipitating agent. In this case, predominantly bipolar P1 paracrystals were obtained. As documented in Fig. 1g, these paracrystals exhibited a central 43-nm-wide bright band (see Fig. 1g, arrowhead) where the staining pattern changes its polarity as indicated by the position of the fine stain lines in the bright/overlap region (see Fig. 1g, arrows). In contrast to

the paracrystals induced by divalent cations which became extremely long (>2 μm), the spermine paracrystals were only up to 1 μm long.

Localization of Cysteines in the ABRM Paramyosin Molecule

To distinguish the NH_2- from the COOH-terminal end of paramyosin by EM, the avidin–biotin system developed by Sutoh *et al.* (1984) was combined with proteolytic digestion of paramyosin. First, the number of sulfhydryl groups was determined by the Ellman method (Ellman, 1959). This method revealed that the ABRM paramyosin molecule contains four cysteine residues, i.e., two per chain. The SH groups of ABRM paramyosin were covalently bound to maleimide–biotin (a thiol-specific reagent containing biotin; Bayer *et al.*, 1985), and the biotinylated protein was subsequently tagged with monomeric avidin (dimensions 5.5 nm × 5.5 nm × 4.1 nm; Green *et al.*, 1971). As illustrated in Fig. 2a, when this preparation was visualized in the EM after glycerol spraying/rotary metal shadowing, the paramyosin molecules were labeled with avidin at two distinct sites: (i) at one end of the molecule (see Fig. 2a, arrowheads; and first and third row in Fig. 2b) and (ii) at about 30 nm from the other end (see Fig. 2a, arrows; and second and third row in Fig. 2b). The first type of label was always more frequent (up to 80% of the labeled molecules) than the second one (5 to 20% of the labeled molecules), indicating different reactivities of the two SH groups.

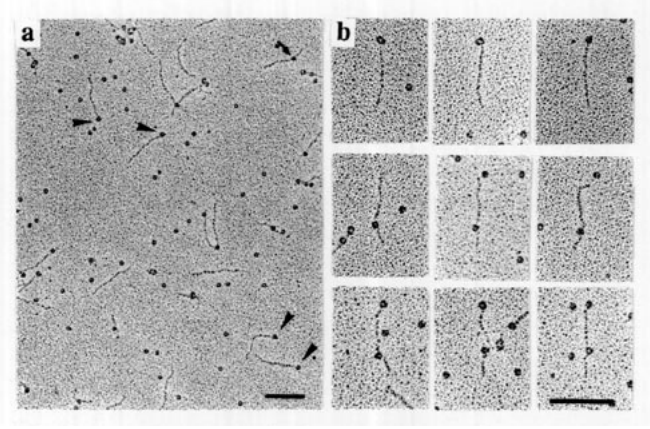

FIG. 2. Avidin–biotin labeling of ABRM paramyosin. (a) General view and (b) gallery of selected examples of biotinylated ABRM paramyosin with bound avidin. The SH groups of ABRM paramyosin were modified with maleimide–biotin and monomeric avidin was bound to the biotinylated protein. The avidin-biotinylated paramyosin complex was then visualized in the EM after glycerol spraying/rotary metal shadowing. Avidin was found associated with paramyosin at two distinct sites: (i) at one end of the molecule (arrowheads in a, and first and third rows in b) and (ii) at about 30 nm from the other end (arrow in a, and second and third row in b). Bars, 100 nm (a–b).

To identify the two avidin–biotin binding sites of ABRM paramyosin in relation to the NH_2- and the COOH-terminal ends of the molecule, paramyosin fragments were produced by carboxypeptidase digestion and labeled with the avidin–biotin system. To obtain paramyosin fragments that could be clearly distinguished from the intact molecule by EM, several digestion conditions were explored. Under mild conditions, (i.e., at 0°C, neutral pH, and incubation times <12 hr), paramyosin treated with either 1% carboxypeptidase G or carboxypeptidase A revealed no significant decrease in molecular weight by SDS–PAGE. However, as documented in Fig. 3a, when the digestion was done with 1% carboxypeptidase G at 32°C in a high-ionic-strength buffer (i.e., 0.6 *M* NaCl, 50 m*M* Tris–Cl, pH 8.0), ABRM paramyosin was progressively cleaved to a 93-kDa fragment (termed CPG93), and after 48 hr of digestion only this fragment was present (see Fig. 3a, lane 5). This condition (i.e., digestion with 1% carboxypeptidase G at 32°C for 48 hr, in 0.6 *M* NaCl, 50 m*M* Tris–Cl, pH 8.0) was chosen to produce CPG93 on a preparative scale. When examined at the EM after glycerol spraying/rotary metal shadowing, this fragment had a length of 110.0 ± 1.2 nm (mean ± SD) (see Table I). Similarly, when paramyosin was digested with 1% carboxypeptidase A at 25°C in the high-ionic-strength buffer (see above), two bands with molecular weights of 85 and 79 kDa (CPA85 and CPA79) started to appear on the SDS–PAGE after 8 hr of digestion. As the digestion proceeded, the native paramyosin was progressively cleaved into these two fragments, and after 24 hr of digestion only these two bands were left by SDS–PAGE (see Fig. 3a, lane 6). Hence, bulk preparation of CPA85 and CPA79 was performed by digestion of ABRM paramyosin with 1% carboxypeptidase A at 25°C for 24 hr. Due to the close similarity of their molecular weights these two fragments were difficult to separate; however, they could be distinguished in the EM by their length. When this preparation was observed in the EM after glycerol spraying/rotary metal shadowing, ~40% of the molecules had a length of 100.0 ± 1.0 nm (mean ± SD) and ~60% were 90.0 ± 1.0 nm (mean ± SD) in length (see Fig. 3b and Table I).

As illustrated in Fig. 3c, when CPG93, CPA85, and CPA79 were labeled with the avidin–biotin system and visualized in the EM after glycerol spraying/rotary metal shadowing avidin was found associated with one end of the molecule. In some cases CPG93 and CPA85 also revealed a second avidin label very close to the other end of the molecule (see Fig. 3b, arrow; and second row in Fig. 3c). As with the paramyosin molecule (see above and Fig. 2) the second type of labeling was observed less frequently (<10% of the labeled molecules). Taken together,

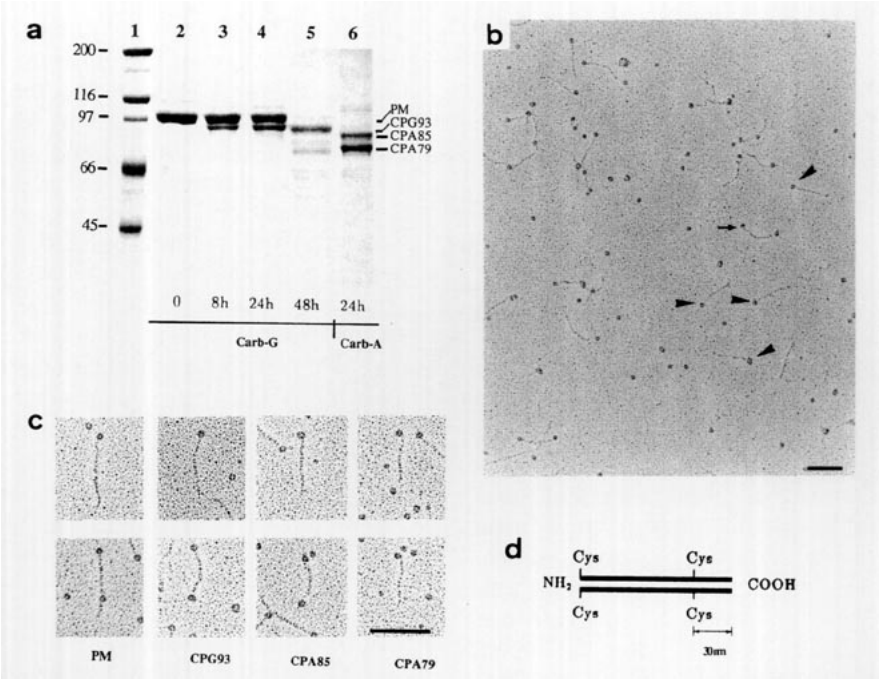

FIG. 3. Carboxypeptidase digestion and avidin–biotin labeling of the carboxypeptidase fragments of ABRM paramyosin. (a) 8% SDS–polyacrylamide gel of the time course digestion of ABRM paramyosin with carboxypeptidase G (lanes 2–5). Digestion with 1% carboxypeptidase G for 48 hr (see Materials and Methods) produces the 93-kDa fragment CPG93 (lane 5). Digestion with 1% carboxypeptidase A for 24 hr (see Materials and Methods) produces the 85- and 79-kDa fragments CPA85 and CPA79 (lane 6). Lane 1, molecular weight standards (myosin, 200 kDa; β-galactosidase, 116 kDa; phosphorylase b, 97 kDa; bovine albumin, 66 kDa; ovalbumin, 45 kDa). (b) General view of the carboxypeptidase A digestion products (as in a, lane 6) of ABRM paramyosin labeled with the avidin–biotin system and visualized in the EM after glycerol spraying/rotary metal shadowing. (c) Gallery of selected examples of ABRM paramyosin (PM) and its carboxypeptidase fragments CPG93, CPA85, and CPA79 labeled with the avidin–biotin system. All the molecules were labeled with avidin at one end (arrowheads in b, and first row in c). A second avidin was also found associated with CPG93 and CPA85 very close to the other end of the molecule (b, arrow, and second row in c). This labeling corresponds to that seen in the native molecule at the second position (at ~30 nm from the other end). (d) Schematic representation of the location of the cysteine residues on the ABRM paramyosin molecule. Bars, 100 nm (b and c).

these results suggested that the cysteine residues of ABRM paramyosin are located pair wise at the NH_2-terminal end of the molecule and at ~30 nm from the COOH-terminal end (see Fig. 3d).

Avidin–Biotin Labeling of Paramyosin Paracrystals

To determine the polarity of paramyosin in *in vitro* assembled paracrystalline arrays, bipolar P1 paracrystals obtained using spermine as the precipitating agent were labeled with the avidin–biotin system and visualized in the EM after negative staining. As illustrated in Fig. 4, avidin–biotin-labeled paracrystals showed marked changes in their staining pattern, which were more pronounced at the ends of the paracrystals probably due to the fact that the paracrystals are tapered at the ends. As the paramyosin paracrystals, depending on the crystallization conditions employed, are highly polymorphic (Cohen *et al.*, 1971), it could be argued that this new staining pattern simply represented a new paracrystal form. However, since spermine-induced paracrystals were used which are less polymorphic, and since all the reactions (i.e., reduction of SH groups, biotinylation, and avidin binding) were performed in the spermine buffer used to form the paracrystals, the changes in the staining pattern of these paracrystals are probably due to the binding of avidin to the paracrystals. In support of this conclusion, the new staining pattern was not observed even after biotinylation of the paracrystals.

As documented in Figs. 5b and 5d, compared with unlabeled controls, the avidin–biotin-labeled paracrystals exhibited: (i) narrowed dark/gap re-

TABLE I
Proteolytic Fragments of ABRM Paramyosin

	Chain weight (kDa)[a]	Molecular length (nm)[b]	Diagram of the fragments[c]
Native PM	100	124.0 ± 1.2	H_2N ●—● COOH
CPG93	93	110.0 ± 1.2	H_2N ●—●
CPA85	85	100.0 ± 1.0	H_2N ●—●
CPA79	79	90.0 ± 1.0	H_2N ●—

[a] Determined by SDS–PAGE.
[b] Determined by glycerol spraying/rotary metal shadowing.
[c] (●) The location of the Cys determined by EM of glycerol sprayed/rotary metal shadowed avidin–biotin-labeled molecules.

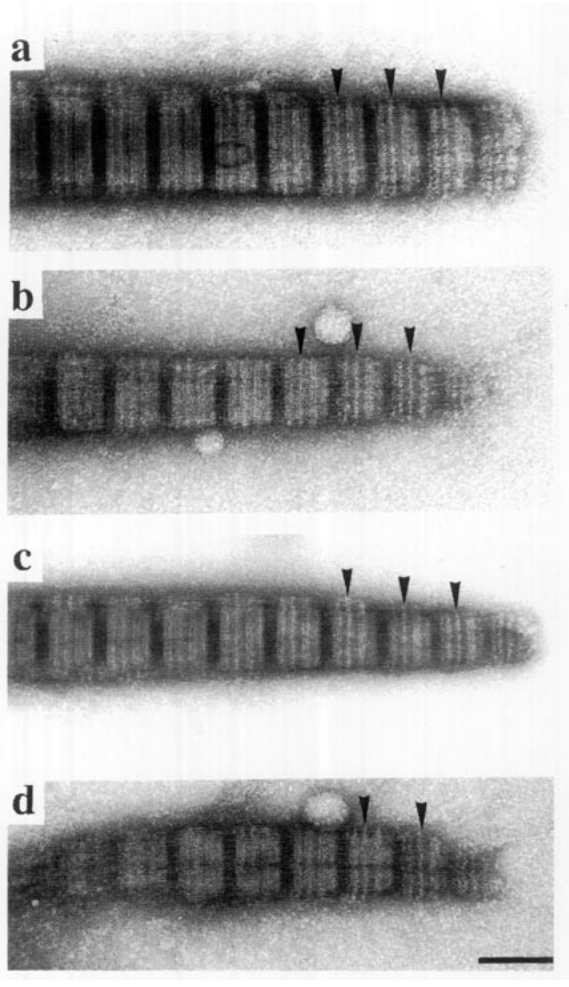

FIG. 4. P1 paracrystals labeled with the avidin–biotin system. ABRM paramyosin paracrystals were formed using spermine as the precipitating agent (see Materials and Methods). The paracrystals were biotinylated with malemide–biotin and monomeric avidin was added to the paracrystal preparation. All the reactions were carried out in the spermine buffer used to form the paracrystals, and the avidin–biotinylated paracrystals were examined by negatively staining in the EM. The avidin–biotinylated paracrystals shown marked changes in their staining pattern after avidin biotinylation (arrowheads). Bar, 100 nm (a–d).

gions at the end of the paracrystal (see Fig. 5d) and (ii) two additional narrow (~5-nm-wide) dark bands in the overlap region surrounding a ~8-nm-wide stain excluding band (see Figs. 4 and 5d, arrowheads) which is centered at ≈30 nm from the left edge of the dark/gap region (left side of the dark/gap region in Fig. 5d). These changes in the staining pattern of the paracrystals can be explained by the association of avidin with the two cysteine residues of paramyosin. Since avidin binds to the NH_2-terminal end of the paramyosin molecule (see above and Fig. 2), and since the dark bands of the P1 paracrystal are gaps between the ends of the molecules where stain accumulates, the width of the dark bands is expected to decrease when avidin (which

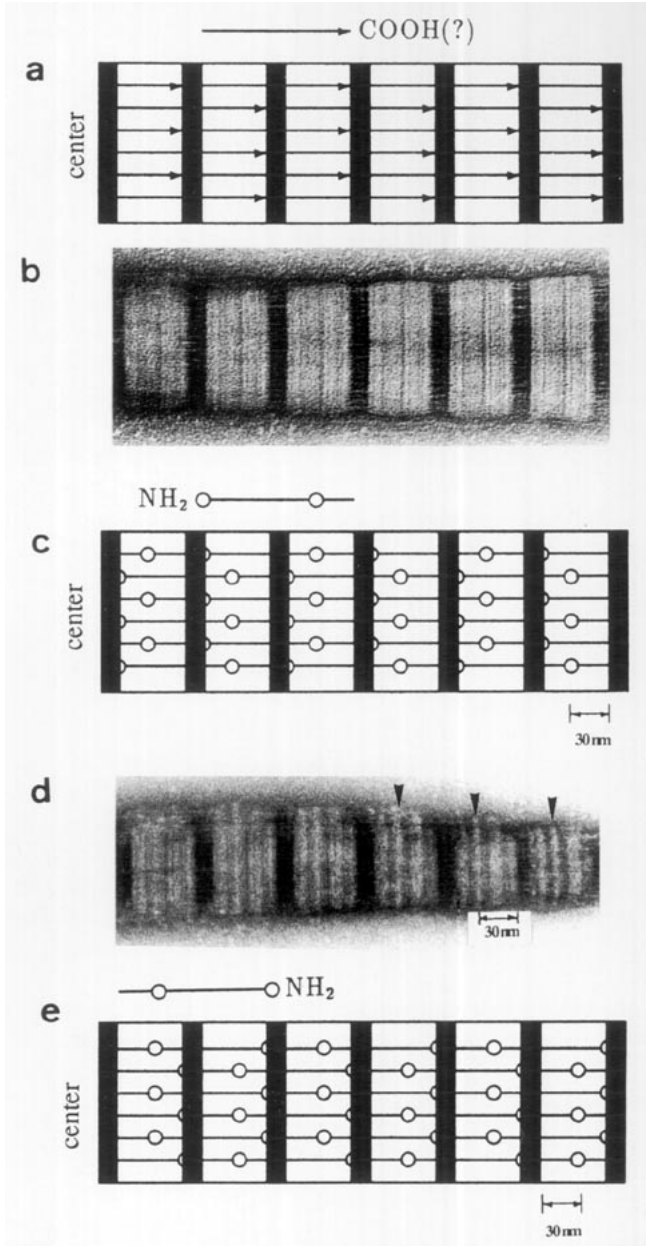

FIG. 5. Comparison of the staining band pattern of avidin-biotinylated paracrystals with control unlabeled paracrystals. (a) Schematic representation of the axial arrangement of paramyosin in the P1 paracrystal (b) proposed by Cohen *et al.* (1971). Paramyosin molecules drawn as 124-nm arrows are staggered by 72.5 nm (the axial repeat of the paracrystal) to produce the dark/bright staining band pattern where the dark bands represent gap between the ends of the molecules, and the light bands regions where the molecules overlap. The orientation of the paramyosin molecules in this model is not known—i.e., it is not known whether the arrowheads indicate the NH_2- or the COOH-terminal end of paramyosin. (c, e) Schematic representations of the expected appearance of the P1 paracrystal for the two possible orientation of paramyosin when the paramyosin molecule is labeled with the avidin–biotin system. The two avidin molecules at the NH_2-terminal end and at 30 nm from the COOH-terminal end of paramyosin are modeled as two open circles. The paramyosin molecules are oriented in a P1 array with their NH_2-terminal end pointing either toward the center (c) or toward the end (e) of the paracrystal. (d) P1 paracrystal labeled with the avidin–biotin system. The paracrystal exhibits narrowed dark/gap regions at the end, and a new bright band (arrowheads) surrounded by two fine dark bands in the overlap region. These changes are consistent with the labeling expected if the NH_2-terminal end of paramyosin points toward the center of the paracrystal (c). Bars, 30 nm (a–e).

excludes stain) binds to the paracrystal. Similarly, the new 8-nm bright band located at 30 nm from the left edge of the dark/gap region (see Fig. 5d, arrowheads) can be interpreted to represent the bound avidin at 30 nm from the COOH-terminal end of paramyosin. In this case, the bound avidin (which excludes stain) is surrounded by dark regions where stain accumulates on either side of the bound avidin. These interpretations suggest that the left edge of the dark/gap region represents the COOH-terminal end of paramyosin which is therefore pointing toward the end of the paracrystal.

As documented in Figs. 5c and 5e, drawing of the expected appearance of the P1 paracrystal for the two possible orientations of paramyosin when the molecule is labeled with avidin can explain the changes observed in the avidin-labeled paracrystal. Accordingly, if the NH_2-terminal end of paramyosin points toward the center of the paracrystal (Fig. 5c), the avidin is expected to bind (i) at the right edge of the dark/gap regions (right side of the black bands in Fig. 5c) and (ii) at 30 nm from the left edge of the dark/gap regions (left side of the black bands in Fig. 5c). On the other hand, if the NH_2-terminal end of paramyosin points toward the end of the paracrystal (Fig. 5e), the avidin would bind (i) at the left edge of the dark/gap regions (left side of the black bands in Fig. 5e) and (ii) at 30 nm from the right edge of the dark/gap regions (right side of the black bands in Fig. 5e). The labeling patterns of the avidin-conjugated paracrystals (Figs. 4 and 5d) are consistent with the labeling expected if the NH_2-terminal end of paramyosin points toward the center of the paracrystal (Fig. 5c).

Comparison of α- and β-Paramyosin Paracrystals also Revealed the Polarity of Paramyosin

An alternative method was used to verify the polarity of paramyosin in the bipolar P1 paracrystals. It consists of comparing the band pattern of paracrystals assembled from proteolytically cleaved paramyosin with those made of the intact molecule. Since attempts to form paracrystals of the carboxypeptidase fragments of ABRM α-paramyosin (i.e., CPG93, CPA85, and CPA79) were unsuccessful, β-paramyosin (a proteolytically cleaved α-paramyosin that has lost a small region at the COOH-terminal end; Yeung and Cowgill, 1976) was isolated from ABRM. As illustrated in Fig. 6a, ABRM β-paramyosin was only by ~4 kDa smaller than the native molecule. In contrast to the carboxypeptidase fragments of α-paramyosin, β-paramyosin readily formed P1 paracrystals (Figs. 6b and 6c). At first glance, the band pattern of the P1 paracrystals made from β-paramyosin looks similar to that of the α-paramyosin paracrystals: compare for example the α-paramyosin paracrystal in Fig. 1c with the β-paramyosin paracrystals in Figs. 6b and 6c. However, more careful inspection of their band patterns revealed some subtle differences at the edges of the dark bands. As illustrated in Fig. 6d, in the P1 paracrystals made from α-paramyosin the two edges of the dark bands look different: the edge facing the end of the paracrystal (i.e., the right edge of the dark bands in Fig. 6d) is sharp, whereas the edge facing the center of the paracrystal (i.e., the left edge of the dark bands in Fig. 6d) appears fuzzy. In contrast, as documented in Fig. 6e, in the β-paramyosin paracrystals both edges of the dark band appear sharp. Thus the fuzzy edge (i.e., the left edge of the dark band in Fig. 6d) of the α-paramyosin paracrystal becomes sharp in the β-paramyosin paracrystal (Fig. 6e). Taken together, these results suggest that the fuzzy edge facing the end of the α-paramyosin paracrystal represents the COOH-terminal end of paramyosin, which is pointing toward the end of the paracrystal. Thus, this result confirms the polarity of paramyosin determined using the avidin–biotin system (see above).

Native Thick Filaments and Paramyosin Core from ABRM

As illustrated in Fig. 7a, when examined in the EM after negative staining, thick filaments isolated form the ABRM of *M. edulis* are extremely large, up to 20 μm in length and ~150 nm in diameter, and revealed a transverse band pattern with an axial periodicity of 14.5 nm. Although ATP was always present during the isolation procedure (condition that minimizes myosin disassembly; Nonomura, 1974), the surface of these filaments exhibits a smooth appearance with no obvious indication of myosin heads. As illustrated in Figs. 7b and 7c, upon washing of these filaments with high-ionic-strength buffer (i.e., 0.4 *M* NaCl, 5 m*M* $MgCl_2$, 1 m*M* ATP, 20 m*M* Mes, pH 6.0) to extract the myosin, they revealed the characteristic Bear–Selby net. Judged from the increased diameter, after this treatment, the paramyosin core appeared to swell (Figs. 7b and 7c; see also Castellani *et al.*, 1983). As in other molluscan thick filaments (Szent-Györgyi *et al.*, 1971; Bennett and Elliott, 1984) the nodes of the Bear–Selby net have a roughly triangular shape (see Figs. 7b and 7c, white arrows). As illustrated in Fig. 7c, one vertex of the triangular nodes points toward the center of the filament where this polarity reverses. This orientation of the Bear–Selby nodes is an indication of the polarity of paramyosin in the native core.

From the knowledge of the polarity of the paramyosin molecules in the P1 paracrystals it is possible to infer the orientation of the molecules in the native core. Since the Bear–Selby net of the native paramyosin core has been explained in terms of axial dis-

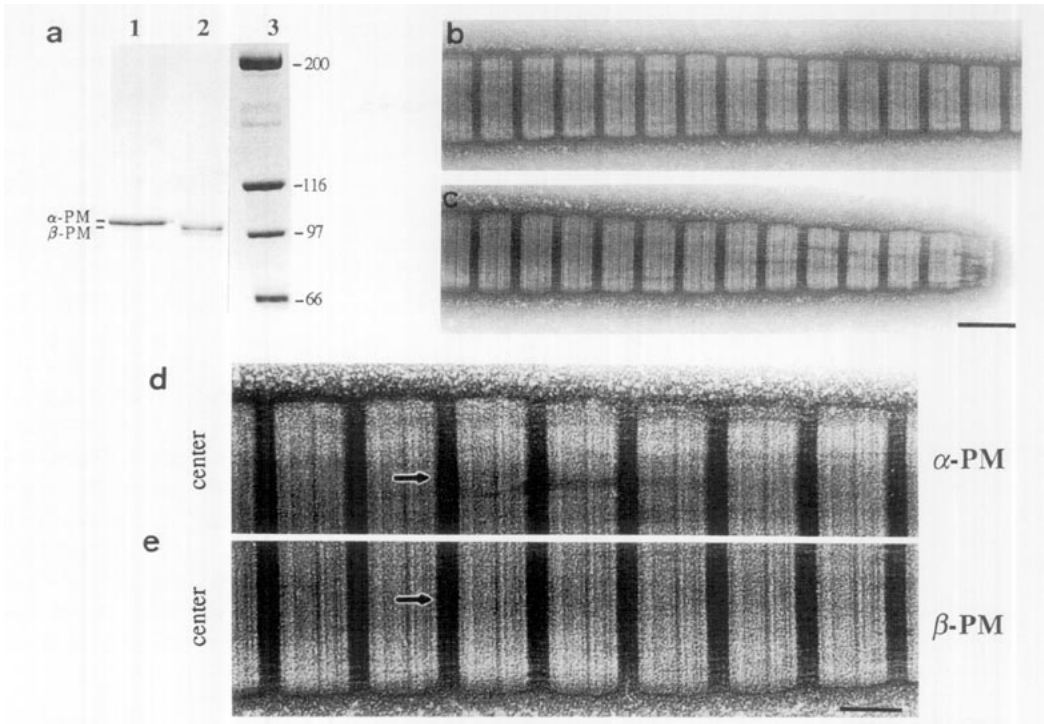

FIG. 6. ABRM α- and β-paramyosins. (a) 5% SDS–polyacrylamide gel of α- and β-paramyosins isolated from ABRM. ABRM β-paramyosin (lane 1) is only ~4 kDa less than the native α-paramyosin. Lane 3, molecular weight standards (myosin, 200 kDa; β-galactosidase, 116 kDa; phosphorylase b, 97 kDa; bovine albumin, 66 kDa (lane 2). (b, c) Negatively stained P1 paracrystals made from β-paramyosin induced using divalent cations as the precipitating agent (see Materials and Methods). ABRM β-paramyosin formed P1 paracrystal similar to those of the intact α-paramyosin (see Fig. 1c). (d, e) Comparison of the staining band pattern of P1 paracrystals made from α- and β-paramyosin (d and e). In the P1 paracrystal from α-paramyosin (d), the two edges of the dark bands look different: the right edge is sharp, whereas the left edge (arrow) appears fuzzy. In contrast, the two edges of the dark band appear sharp in the β-paramyosin paracrystal (e). This difference between the α- and the β-paramyosin P1 paracrystal in the edge of the dark/gap region facing the center of the paracrystal (arrow) indicates that this edge represent the COOH-terminal end of paramyosin, which it is therefore pointing toward the end of the paracrystal. Bars, 100 nm (b and c) and 50 nm (d and e).

placement of subfilaments having the P1 paracrystalline packing (Cohen *et al.*, 1971) (see Fig. 1f), and since paramyosin assembles with the NH_2-terminal end pointing toward the center of the bipolar P1 paracrystals (see above), it follows that paramyosin may assemble with its NH_2-terminal end pointing toward the center of the native paramyosin filament. The following observations support this notion: (i) the base of the triangular Bear-Selby nodes which coincides with the 14.5-nm transverse band of the thick filament yield a sharp appearance (see Fig. 7b, white arrows) similar to the edge of the dark band of the P1 paracrystal that faces the end of the paracrystal (see Fig. 6d, right edge of dark bands) and (ii) the Bear–Selby nodes have also been described to having a sharp and a fuzzy edge (Bennett and Elliott, 1984), with the orientation of these two edges corresponding to that described here for the edges of the dark band of the P1 paracrystals, i.e., the edge facing the end of the paracrystal is sharp (see Fig. 6d, right edge of dark bands), whereas the edge facing the center of the paracrystal is fuzzy (see Fig. 6d, left edge of dark bands).

DISCUSSION

Location of Cysteines by the Avidin–Biotin System

The amount of cysteine residues of ABRM paramyosin determined here by the Ellman method (i.e., two cysteine residues per chain) is consistent with that found in the adductor muscle of the clam *Mercenaria mercenaria* (Cowgill, 1974). It also agrees with the number of cysteines from the amino acid sequences of the few paramyosins thus far cloned and sequenced (i.e., from the nematode *C. elegans*, Kagawa *et al.*, 1989; from the dog heartworm parasite *D. immitis*, Limberger and McReynolds, 1990; and from *Drosophila melanogaster*, Becker and Bernstein, 1990). One exception is the amino acid sequence of *Shistosoma mansoni* paramyosin which reveals only one cysteine residue per chain (Laclette *et al.*, 1991). Although there are four cysteines per ABRM paramyosin molecule, only two sites were labeled with the avidin–biotin system. Thus, the cysteine residues in the ABRM paramyosin occur as two pairs, one pair is located in the NH_2-terminal end and the other at ~30 nm from

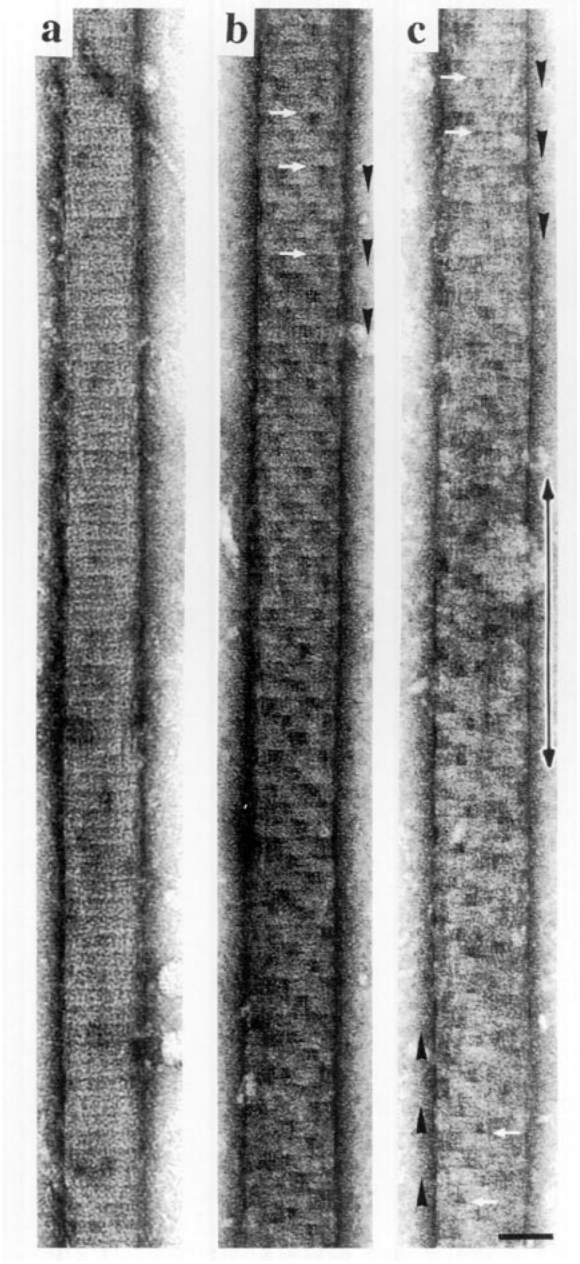

FIG. 7. Native thick filaments from ABRM. (a) Negatively stained native thick filament isolated from ABRM showing the 14.5-nm axial repeat. (b, c) Negatively stained native paramyosin core showing the characteristic Bear–Selby net. The Bear–Selby nodes have a roughly triangular shape (white arrows in b and c) with one vertex pointing toward the center of the filament (indicated by the arrowheads next to the filaments in b and c). This polarity reverses at the center of the filament (arrowed bar in c). Bar, 50 nm (a–c).

the COOH-terminal end of the molecule (see Fig. 3d). Similarly, Cowgill, (1974) based on the analysis of digestion products, found that the four SH groups of *Mercenaria* paramyosin where located pairwise at the NH_2-terminal end and at ~40 nm from the COOH-terminal end of the molecule. As in the ABRM and *Mercenaria* paramyosin molecules, the amino acid sequences of paramyosin from *C. elegans* (Kagawa *et al.*, 1989) and *D. immitis* (Limberger and McReynolds, 1990) also revealed one of the cysteine residue at ~¼ from the COOH-terminal end of the molecule. The other cysteine is located at residue 127 of the *C. elegans* paramyosin sequence and at residue 105 of the *D. immitis* paramyosin sequence. In the amino acid sequences of paramyosin from *Drosophila* (Becker and Bernstein, 1990) and *Shistosoma* (Laclette *et al.*, 1991) the location of the cysteine residues is less conserved. They occur at residues 368 and 784 in *Drosophila* paramyosin (total amino acid residues = 879) and at residue 750 in *Shistosoma* paramyosin (total amino acid residues = 866).

The location of the cysteine ABRM groups in the paramyosin molecule suggested that paramyosin is probably a homodimer. However, the avidin-labeling method does not have enough resolution to reveal minor differences between the two chains. Evidence in favor of both identity and difference of the two paramyosin chains have been reported. On the one hand, analysis of digestion products of paramyosin suggested that paramyosin is a homodimer (Cowgill 1974; Weisel and Szent-Györgyi, 1975). On the other hand, based on the amino acid sequence around the four cysteine residues of paramyosin from the smooth adductor muscle of scallop, Walker and Stewart (1975) concluded that there were two different types of chains. This latter result could be explained by tissue heterogeneity which has been reported to occur in this muscle (Morita and Kondo, 1982). Another possibility is the existence of paramyosin isoforms, which at least in the case of *C. elegans* has recently been demonstrated (Deitiker and Epstein, 1993).

The COOH-Terminal End of Paramyosin Is Important for Assembly

Similar to myosin, where its solubility and assembly properties are controlled by a small region of its COOH-terminal end (Sinard *et al.*, 1990; Atkinson and Stewart, 1991), the COOH-terminal end of paramyosin appears to play an important role in the assembly of this molecule. Whereas β-paramyosin, i.e., α-paramyosin which has lost a ~4-kDa segment at its COOH-terminal end, formed paracrystals very similar to those of the intact molecule (i.e., α-paramyosin), the three carboxypeptidase fragments of ABRM paramyosin CPG93, CPA85, and CPA79 did not form P1 paracrystals under the ionic conditions explored here (see Materials and Methods). Since the CPG93 fragment is only ~3 kDa smaller than β-paramyosin (i.e., ~27 amino acid residues), and since CPG93 is only ~14 nm shorter than the native molecule, it is conceivable that the region controlling the assembly of ABRM paramyosin is ~27 residues long and may be located at less

than 14 nm from the COOH-terminal end of the molecule. Consistent with these conclusions, at least five missense mutations affecting filament formation were located in a 38-residue-long region of the COOH-terminal end of *C. elegans* paramyosin (Gengyo-Ando and Kagawa, 1991).

Polarity of Paramyosin

The structure of the thick filament from molluscan muscles has been the subject of many structural studies (reviewed by Bennett and Elliott, 1987). These studies have shown that paramyosin forms the paracrystalline core of the filament with myosin decorating its surface. However, the molecular packing of paramyosin in the core and its polarity in the native filament have remained elusive. In the present investigation, the polarity of paramyosin in the P1 paracrystals was determined using two different experimental approaches: (i) avidin–biotin labeling of paracrystals and (ii) comparison of the transverse band-like staining pattern of paracrystals made of α-paramyosin (intact protein) and β-paramyosin (a proteolytically cleaved α-paramyosin that has lost a small segment at its COOH-terminal end). Both methods have revealed that paramyosin assembles with its NH_2-terminal end pointing toward the center of the bipolar paracrystals. Since the P1 paracrystal has been shown to be the basic paracrystalline array yielding for the Bear–Selby net of the native filament (Cohen *et al.*, 1971), the polarity of paramyosin in the P1 paracrystals was assumed to also represent the orientation of paramyosin in the native filament. Accordingly, paramyosin assembles with its NH_2-terminal end pointing toward the center of the bipolar thick filament. This result is in agreement with that reported by Weisel (1975).

Paramyosin–Paramyosin Interactions

As documented in Fig. 8, the axial array of the paramyosin molecules in the bipolar P1 paracrystal yields three possible types of lateral interactions between paramyosin molecules: (i) parallel interactions with an N-C type overlap of ~52.5 nm, (ii) antiparallel interactions with ~43-nm N–N-type overlap, and (iii) antiparallel interactions with ~43-nm C–C-type overlap. The first type of interaction was initially described by Cohen *et al.* (1971) when the axial array of paramyosin in synthetic paracrystals was determined. However, due to the uncertainty of the orientation of the molecules in the paracrystal, it was difficult to decide whether the 43-nm-long overlap at the center of bipolar P1 paracrystals was an N–N or a C–C type. Recently, Kagawa *et al.* (1989) have calculated the electrostatic interactions of the amino acid sequence of paramyosin from *C. elegans* and found that all these

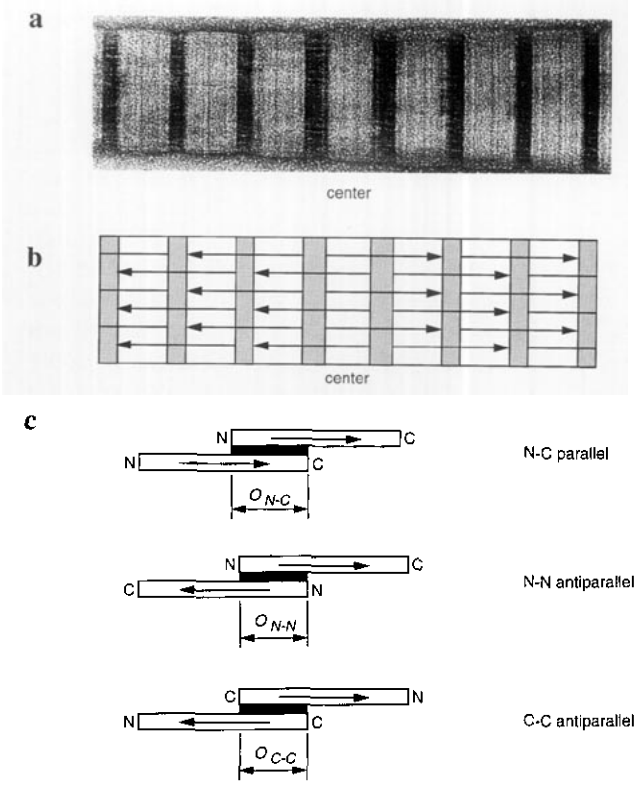

FIG. 8. Axial arrangement of paramyosin molecules in the bipolar P1 paracrystal. (a) Bipolar P1 paracrystal induced using spermine as the precipitating agent (see Materials and Methods). The paracrystal exhibits a central 43-nm-wide bright band where the polarity of the transverse band-like staining pattern reverses. (b) Schematic representation of the axial arrangement of paramyosin molecules in the bipolar P1 paracrystal adapted from Cohen *et al.* (1971). The paramyosin molecules drawn as arrows are staggered to produce the dark/bright staining band pattern. The dark bands represent gap between the ends of the molecules, and the bright bands are regions where the molecules laterally overlap. The orientation of the paramyosin molecules reverses at the center of the bipolar paracrystal. (c) Diagram of the three possible modes of interactions between paramyosin molecules inferred from the axial array of paramyosin in the bipolar P1 paracrystal (b): (i) parallel N–C type with a 52.5-nm N–C overlap (o_{N-C}), (ii) antiparallel N–N type with a 43-nm N–N overlap (o_{N-N}), and (iii) antiparallel C–C type with a 43-nm C–C overlap (o_{C-C}). Since paramyosin assembles in the bipolar P1 paracrystal with the NH_2-terminal end pointing toward the center of the filament, the N–N type of antiparallel interaction occurs at the center of the bipolar P1 paracrystal.

three type of interactions were favorable. From the knowledge of the polarity of the paramyosin molecules determined in the present work, we can now conclude that the N–N type of antiparallel interaction occurs at the center of bipolar P1 paracrystals.

Myosin–Paramyosin Interactions

Kagawa *et al.* (1989) also calculated the electrostatic interactions between the amino acid sequence of paramyosin and that of the myosin rod, and thereby found several possible modes of both parallel and antiparallel arrangements between the two

types of molecules. Based on their calculations, these authors proposed a model for the most stable arrangement of myosin and paramyosin in the thick filament in which the two types of molecules interact in a parallel fashion. As a consequence, paramyosin had to be oriented with its COOH-terminal end pointing toward the center of the filament. While the myosin–paramyosin arrangement proposed in this model could in principle be possible in the center of the filament where both parallel and antiparallel interactions between myosin and paramyosin might occur, the polarity of the paramyosin molecules in this model is the opposite of that reported here—i.e., the NH_2-terminal end of the paramyosin molecules pointing toward the center of the filament. This orientation of paramyosin implies that at the ends of the native filament myosin and paramyosin assemble with different polarities, i.e., the NH_2-terminal end of the paramyosin molecules points toward the center, whereas the NH_2-terminal end of the myosin molecules (i.e., the myosin heads) points toward the end of the filament. Therefore, the assembly of myosin and paramyosin at the end of the thick filament would be in an antiparallel fashion, where the NH_2-terminal end of paramyosin interacts with the COOH-terminal end of myosin.

In the case of antiparallel arrangements of myosin and paramyosin molecules, Kagawa *et al.* (1989) predicted four possible modes of interactions involving amino acid shifts $s = -196$, 0, $+283$, and $+388$ residues. As illustrated in Fig. 9a, a value of $s = -196$ residues corresponds to an arrangement where the COOH-terminal end of paramyosin is staggered by ~29 nm relative to the NH_2-terminal end of the myosin rod. This spacing, which corresponds to the axial stagger of adjacent Bear–Selby nodes (i.e., $\frac{2}{5} \times 72.5$ nm), is a fundamental repeat in the native thick filament. As was demonstrated by Cohen et al. (1971), the paramyosin core can be described made up of subfilaments corresponding to the P1 array. Accordingly, axial displacements of subfilaments by 29 nm produces the Bear–Selby net. The nodes of the Bear–Selby net represent therefore the dark bands of the P1 array, which correspond to the gap regions between the ends of adjacent paramyosin molecules. If myosin is placed with the antiparallel type of interaction involving $s = -196$ residues (Fig. 9a) in a paramyosin subfilament having the axial P1 arrangement (Fig. 9b), and if the subfilaments are axially shifted by 29 nm to build the Bear–Selby net, the model shown in Fig. 9c is generated (adapted from Cohen, 1982). In this model the myosin heads coincide roughly with the dark band of the subfilaments. This overlap of the myosin heads with the gap regions of the neighboring subfilament could explain why the Bear–Selby net of

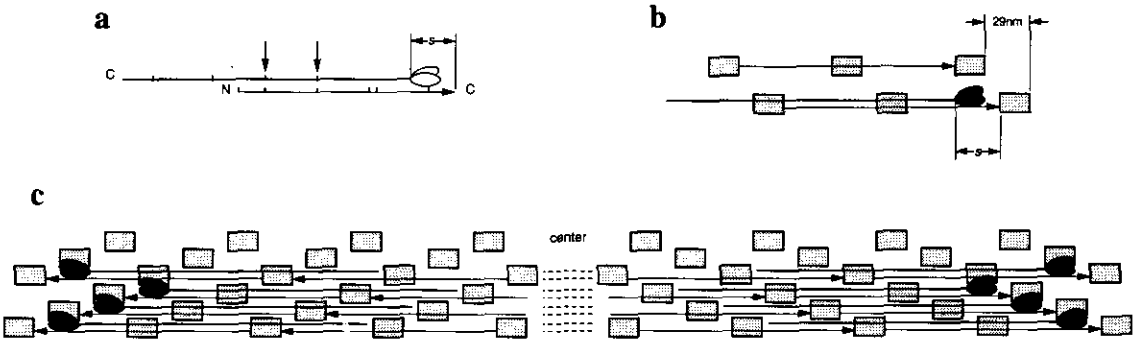

FIG. 9. Schematic representation of one possible molecular arrangement of myosin and paramyosin molecules in the native thick filament of molluscan smooth muscle. (a) Diagram of the antiparallel lateral arrangement of myosin and paramyosin molecules predicted by Kagawa *et al.* (1989) for a stagger between the two amino acid sequences of $s = -196$ residues, in which the COOH-terminal end of a paramyosin molecule (arrowhead) is shifted away from the NH_2-terminal end of the myosin rod by ~29 nm. The vertical bars along the two molecules indicate the positions of "skip" residues, which are amino acid residues that interrupt the heptad peptide repeat and are believed to represent local distortions that modulate the pitch of the two-stranded α-helical coiled-coil (McLachlan and Karn, 1982, 1983; Kagawa *et al.*, 1989). In this arrangement (i.e., for $s = -196$ residues), two of the skip residues of the paramyosin sequence coincide with two skip residues of the myosin rod sequence (arrows), an arrangement which might strengthen the interaction between the two molecules. (b) Diagram of two subfilaments of paramyosin in which the paramyosin molecules (drawn as arrows) have the axial arrangement of the P1 paracrystalline packing. The rectangles correspond to the dark/gap region of the P1 paracrystal. To simplify the model only one paramyosin molecule in each subfilament is drawn. The arrowheads represent the COOH-terminal end of the paramyosin molecules which point toward the end of the subfilament. In the subfilament on the bottom, a myosin molecule is drawn interacting with paramyosin with the antiparallel mode of interaction shown in a (i.e., for $s = -196$ residues). (c) A possible model for the molecular arrangement of myosin on the Bear–Selby net of the thick filament. The Bear–Selby net is generated by shifting subfilaments having the arrangement of myosin and paramyosin as shown in b by 29 nm (i.e., $\frac{2}{5} \times 72.5$ nm). In this model the myosin heads coincide roughly with the Bear–Selby nodes. To simplify the model only one paramyosin molecule per node and four myosin molecules are drawn. There will probably be three or four (2-nm-wide) paramyosin molecules per node on the surface of the paramyosin core (from ABRM the width of the nodes is ~6 nm). The actual number of myosin molecules per node is unknown, but values up to three myosin molecules per node have been calculated (Elliott, 1974).

the native thick filament is seen only after selective extraction of myosin. For simplicity, only one myosin molecule per node is drawn in this model, but the actual number of myosin molecules in the thick filament remains unknown. This number appears to depend on the diameter of the thick filament, and values up to three myosin molecules per node have been calculated (Elliott, 1974). Also, in this model only the interaction of myosin with paramyosin involving $s = -196$ is emphasized. Other type of myosin–paramyosin interactions can be depicted from this model. For example, the interactions between a myosin molecule and the paramyosin molecule of the neighboring subfilament (see Fig. 9b), in which there is a maximum overlap between the two molecules, would correspond to the arrangement predicted by Kagawa *et al.* (1989), i.e., $s = 0$ residue.

Structure of Molluscan Thick Filaments and "Catch" Theories

The molecular packing of myosin and paramyosin molecules in the thick filament of molluscan muscles has been related to the unusual contractile activity of some of these muscles, known as the "catch" state, in which tension has to be maintained for a long period of time with little expenditure of energy (see review by Twarog, 1979). In the catch state, although ATP is present, the myosin heads ("crossbridges") are attached to actin and are cycling very slowly. It has been proposed that changes in the intermolecular interaction between the myosin rods and paramyosin and/or myosin in the thick filament influence the rate of crossbridge cycling in catch muscles (Cohen, 1982; Cohen and Castellani, 1988). Furthermore, the findings that both the ABRM myosin rod domain (Castellani and Cohen, 1987) and the paramyosin molecule (Achazi, 1979; Cooley *et al.*, 1979; Castellani and Cohen, personal communication) can be phosphorylated *in vitro* have led to speculations that some specific changes in the mutual interactions of these molecules may occur upon phosphorylation and that the catch state may be mediated by phosphorylation (Cohen, 1982; Cohen and Castellani, 1988; Castellani and Cohen, 1992). The model shown in Fig. 9c, where the COOH-terminal region of paramyosin—which contains the phosphorylation site(s) (located at less than 30 nm from the COOH-terminal end; Panté, Castellani, and Cohen, unpublished results) and controls the solubility and assembly properties of paramyosin (see above)—is in close contact with the myosin heads, would support this hypothesis.

In summary, determination of the polarity of the paramyosin molecules within the P1 paracrystals reported here allows one to infer that in the native thick filaments of molluscan muscles paramyosin may assemble with the same orientation (i.e., with the NH_2-terminal end pointing toward the center of the filament). This assumption, and the knowledge of the most favorable modes of interactions between myosin and paramyosin as calculated by Kagawa *et al.* (1989), allow us to extent the model of Cohen (1982) for the coassembly of myosin and paramyosin in the thick filament which has functional implications (Fig. 9c). Although there is evidence for the specific interaction between myosin and paramyosin (Szent-Györgyi *et al.*, 1971; Nonomura, 1974; Epstein *et al.*, 1975, 1976), more information is required to derive a more detailed model of the molecular organization of these two proteins within the thick filament.

I thank Dr. C. Cohen, in whose laboratory this work was performed, for continued advice and support. I am grateful to Dr. L. Castellani, Dr. B. Elliott, Dr. A. Szent-Györgyi, and Dr. P. Vibert for many helpful suggestions during the progress of this project and to Dr. U. Aebi for critical reading of the manuscript. Ms. H. Frefel and Ms. M. Zoller are thanked for their expert photographic work. This work was supported by grants from the National Institutes of Health AR17346 and the Muscular Dystrophy Association (to C. Cohen) and the National Science Foundation MCB 90-0746 (to P. Vibert and C. Cohen).

REFERENCES

Achazi, R. K. (1979) Phosphorylation of molluscan paramyosin, *Pfluegers Arch.* 379, 19–27.

Atkinson, S. J., and Stewart, M. (1991) Molecular basis of myosin assembly: Coiled-coil interactions and the role of charge periodicities, *J. Cell Sci.* 14 (Suppl.), 7–10.

Bayer, E. A., Zalis, M. G., and Wilchek, M. (1985) T3-(N-Maleimido-propionyl) biocytin: A versatile thiol-specific biotinylating agent, *Anal. Biochem.* 149, 529–536.

Bear, R. S., and Selby, C. C. (1956) The structure of paramyosin fibrils according to X-ray diffraction, *J. Biophys. Biochem.* 2, 55–69.

Becker, K. D., and Bernstein, S. I. (1990) cDNA sequence and analysis of expression of the paramyosin gene of *Drosophila melanogaster*, *J. Cell Biol.* 111, 287a.

Bennett, P., and Elliott, A. (1981). The structure of the paramyosin core in molluscan thick filaments, *Muscle Res. Cell Motil.* 2, 65–81.

Bennett, P. M., and Elliott, A. (1984) "Splicing" of paramyosin filaments, *J. Mol. Biol.* 175, 103–109.

Bennett, P., and Elliott, A. (1987) Molluscan paramyosin filaments, *in* Squire, J., and Vibert, P. (Eds.), Fibrous Protein Structure, pp. 389–421, Academic Press, New York.

Bradford, M. M. (1976) A rapid and sensitive method for the quantitation of microgram quantities of protein utilizing the principle of protein-dye binding, *Anal. Biochem.* 72, 291–323.

Caspar, D. L. D., Cohen, C., and Longley, W. (1969) Tropomyosin: Crystal structure, polymorphism and molecular interactions, *J. Mol. Biol.* 41, 87–107.

Castellani, L., and Cohen, C. (1987) Myosin rod phosphorylation and the catch state of molluscan muscle, *Science* 235, 334–447.

Castellani, L., and Cohen, C. (1992) A calcineurin-like phosphatase is required for catch contraction, *FEBS* 309, 321–326.

Castellani, L., and Vibert, P. (1992) Location of paramyosin in relation to the subfilaments within the thick filaments of scallop striated muscle, *J. Muscle Res. Cell Motil.* 13, 174–182.

Castellani, L., Elliott, B. W., Jr., and Cohen, C. (1988) Phospho-

rylatable serine residues are located in a non-helical tailpiece of a catch muscle myosin, *J. Muscle Res. Cell Motil.* 9, 533–540.

Castellani, L., Vibert, P., and Cohen, C. (1983) Structure of myosin/paramyosin filaments from a molluscan smooth muscle, *J. Mol. Biol.* 167, 853–872.

Cohen, C. (1982) Matching molecules in the catch mechanism, *Proc. Natl. Acad. Sci. USA* 79, 3176–3178.

Cohen, C., and Castellani, L. (1988) New perspective on catch, *Comp. Biochem. Physiol.* 91C, 31–33.

Cohen, C., and Holmes, K. C. (1963) X-ray diffraction evidence for α-helical coiled-coils in native muscles. *J. Mol. Biol.* 6, 423–432.

Cohen, C., Szent-Györgyi, A. G., and Kendrick-Jones, J. (1971) Paramyosin and the filaments of molluscan "catch" muscles. I. Paramyosin: Structure and assembly, *J. Mol. Biol.* 56, 223–237.

Cooley, L. B., Johnson, W. M., and Krause, S. (1979) Phosphorylation of paramyosin and its role in the catch mechanism, *J. Biol. Chem.* 254, 2195–2198.

Cowgill, R. W. (1974) Location and properties of sulfhydryl groups on the muscle protein paramyosin from *Mercenaria mercenaria, Biochemistry* 13, 2467–2474.

Crowther, R. A., Padron, R., and Craig, R. (1985) Arrangement of the heads of myosin in relaxed thick filaments from tarantula muscle, *J. Mol. Biol.* 184, 429–439.

Deitiker, P. R., and Epstein, H. F. (1993) Thick filaments substructures in *Caenorhabditis elegans:* Evidence for two populations of paramyosin, *J. Cell Biol.* 123, 303–311.

Dover, S. W., and Elliott, A. (1979) Three-dimensional reconstruction of a paramyosin filament, *J. Mol. Biol.* 132, 340–341.

Elliott, A., and Bennett, P. M. (1984) Molecular organization of paramyosin in the core of molluscan thick filaments, *J. Mol. Biol.* 176, 477–493.

Elliott, G. F. (1964) Electron microscopy studies of the structure of the filaments in the opaque adductor muscle of the oyster *Crassostrea angulata, J. Mol. Biol.* 10, 489–104.

Ellman, G. L. (1959) Tissue sulfhydryl groups, *Arch. Biochem. Biophys.* 82, 70–77.

Epstein, H. F., Aronow, B. J., and Harriet, E. H. (1975) Interaction of myosin and paramyosin, *J. Supramol. Struct.* 3, 354–360.

Epstein, H. F., Aronow, B. J., and Harriet, E. H. (1976) Myosin-paramyosin cofilaments: enzymatic interactions with F-actin, *Proc. Natl. Acad. Sci. USA* 73, 3015–3019.

Epstein, H. F., Berliner, G. C., Casey, D. L., and Ortiz, I. (1988) Purified thick filaments from the nematode *Caenorhabditis elegans:* Evidence for multiple proteins associated with core structures, *J. Cell Biol.* 106, 1985–1995.

Gengyo-Ando, K., and Kagawa, H. (1991) Single charge changes on the helical surface of the paramyosin rod dramatically disrupts thick filament assembly in *Caenorhabditis elegans, J. Mol. Biol.* 219, 429–441.

Green, N. M., Konieczny, L., Toms, E. J., and Valentine, R. C. (1971). The use of bifunctional biotinyl compounds to determine the arrangement of subunits of avidin, *Biochem. J.* 125, 781–791.

Hall, C. E., Jakus, M. A., and Schmitt, F. O. (1945) The structure of certain muscle fibrils as revealed by the use of electron stains, *J. Appl. Phys.* 16, 459–465.

Hodge, A. J. (1952) A new type of periodic structure obtained by re-constitution of paramyosin from acid solutions, *Proc. Natl. Acad. Sci. USA* 38, 850–855.

Johnson, W. H., Kahn, J. S., and Szent-Györgyi, A. G. (1959) Paramyosin and contraction of "catch muscles," *Science* 130, 160–161.

Kagawa, H., Gengyo, K., McLachlan, A. D., Brenner, S., and Karn, J. (1989) Paramyosin gene (unc-15) of *Caernohabditis elegans:* Molecular cloning, nucleotide sequence and models for thick filament structure, *J. Mol. Biol.* 207, 311–333.

Kensler, R. W., and Levine, R. J. C. (1982) An electron microscopic and optical diffraction analysis of the structure of *Limulus* thick filaments, *J. Cell Biol.* 92, 443–451.

Laclette, J. P., Landa, A., Arcos, L., Willms, K., Davis, A. E., and Shoemaker, C. B. (1991) Paramyosin is the *Schistosoma mansoni* (trematoda) homologue of antigen B from *Taenia solium* (cestoda), *Mol. Biochem. Parasitol.* 44, 287–296.

Laemmli, U. K. (1970) Cleavage of structural proteins during assembly of the head of bacteriophage T4, *Nature* 227, 680–685.

Levine, R. J. C., Elfvin, M., Dewey, M. M., and Walcott, B. (1976) Paramyosin in invertebrate muscles II. Content in relation to structure and function, *J. Cell Biol.* 71, 273–279.

Levine, R. J. C., Kensler, R. W., Stewart, M., and Haselgrove, J. C. (1982) Molecular organization of *Limulus* thick filaments, *in* Twarog, B. M., Levine, R. J. C., and Dewey, M. M. (Eds.), Basic Biology of Muscles: A Comparative Approach, pp. 37–52, Raven Press, New York.

Levine, R. J. C., Chantler, P. D., and Kensler, R. W. (1988) Arrangement of myosin heads on *Limulus* thick filaments, *J. Cell Biol.* 107, 1739–1747.

Limberger, R. J., and McReynolds, L. A. (1990) Filarial paramyosin: cDNA sequences from *Dirofilaria immitis* and *Onchocera volvulus, Mol. Biochem. Parasitol.* 38, 271–280.

Lowry, S., Kucera, J., and Holtzer, A. (1963) On the structure of the paramyosin molecule, *J. Mol. Biol.* 7, 234–244.

Lowry, O. H., Rosenbrough, N. J., Farr, A. J., and Randall, R. J. (1951) Protein measurement with the folin phenol reagent, *J. Biol. Chem.* 193, 265–275.

McLachlan, A. D., and Karn, J. (1982) Periodic charge distributions in myosin rod amino acid sequence match cross-bridge spacings in muscle, *Nature* 299, 226–230.

McLachlan, A. D., and Karn, J. (1983) Periodic features in the amino acid sequence of nematode myosin rod, *J. Mol. Biol.* 164, 605–626.

Morita, F., and Kondo, S. (1982) Regulatory light chain contents and molecular species of myosin in catch muscle of scallop, *J. Biochem.* 92, 977–983.

Nonomura, Y. (1974) Fine structure of the thick filament in molluscan catch muscle, *J. Mol. Biol.* 88, 445–455.

Phillips, G. N., Jr., Cohen, C., and Stewart, M. (1987) A new crystal form of tropomyosin. Preliminar X-ray diffraction analysis, *J. Mol. Biol.* 195, 219–223.

Shotton, D. M., Burke, B. E., and Branton, D. (1979) The molecular structure of human erythrocytes spectrin: Biophysical and electron microscopic studies. *J. Mol. Biol.* 131, 303–329.

Sinard, J. H., Rimm, D. L., and Pollard, T. D. (1990) Identification of functional regions on one tail of *Acanthamoeba* myosin-II using recombinant fusion proteins. II. Assembly properties of tails with NH_2- and COOH-terminal deletions, *J. Cell Biol.* 111, 2417–2426.

Squire, J. (1972) General model of myosin filaments structure. III. Molecular packing arrangements in myosin filaments, *J. Mol. Biol.* 77, 291–323.

Stafford. W. F., and Yphantis, D. A. (1972) Existence and inhibition of hydrolytic enzymes attacking paramyosin in myofibrillar extracts of *Mercenaria mercenaria, Biochem. Biophys. Res. Commun.* 49, 848–854.

Sutoh, K., Yamamoto, K., and Wakabayashi, T. (1984) Electron

microscopic visualization of the SH_1 thiol of myosin by the use of an avidin-biotin system, *J. Mol. Biol.* **178**, 323–339.

Szent-Györgyi, A. G., Cohen, C., and Kendrick-Jones, J. (1971) Paramyosin and the filaments of molluscan catch muscles: II. Native filaments: Isolation and characterization, *J. Mol. Biol.* **56**, 239–258.

Twarog, B. M. (1979) The nature of catch and its control, *in* Pepe, F. A., Sanger, J. W., and Nachmias, V. T. (Eds.), Motility in Cell Function, pp. 231–241. Academic Press, New York.

Vibert, P., and Craig, R. (1983) Electron microscopy and image analysis of myosin filaments from scallop striated muscle, *J. Mol. Biol.* **165**, 303–320.

Walker, I. D., and Stewart, M. (1975) Paramyosin: Chemical evidence for chain heterogeneity, *FEBS Lett.* **58**, 16–18.

Weisel, J. W. (1975) Paramyosin segments: Molecular orientation and interactions in invertebrate muscle thick filaments, *J. Mol. Biol.* **98**, 675–681.

Weisel, J. W., and Szent-Györgyi, A. G. (1975) The coiled-coil structure: identity of the two chains of *Mercenaria* paramyosin, *J. Mol. Biol.* **98**, 665–673.

Yeung, A. T., and Cowgill, R. W. (1976) Structural difference between α-paramyosin and β-paramyosin of *Mercenaria mercenaria*, *Biochemistry* **15**, 4654–4659.